



Experimental study on cutting temperature and cutting force in dry turning of titanium alloy using a non-coated micro-grooved tool

J. Xie ^{*}, M.J. Luo, K.K. Wu, L.F. Yang, D.H. Li

School of Mechanical & Automotive Engineering, South China University of Technology, Guangzhou 510640, China



ARTICLE INFO

Article history:

Received 16 January 2013

Received in revised form

23 May 2013

Accepted 24 May 2013

Available online 31 May 2013

Keywords:

Micro-grooved tool

Cutting temperature

Cutting force

Dry turning

Titanium alloy

ABSTRACT

Various non-coated micro-grooves with 7–149 μm in depth and 0.14–0.50 in aspect ratio are proposed on tool rake surfaces along cutting chip flowing. The objective is to understand how the micro-groove shape and size influence cutting temperature and cutting force in dry turning of titanium alloy. First, the micro-grinding with a diamond wheel V-tip was employed to fabricate accurate and smooth micro-grooves; then dry turning experiments were performed with regard to material removal rate; finally, cutting temperature, cutting force and tool wear were investigated. It is shown that these micro-grooves patterned on tool rake surface contribute to decreasing cutting chip frictions and excluding cutting heat. The micro-grooved tool decreases cutting temperature by 103 °C and more against traditional plane tool. The predicted cutting tip temperature reaches about 1322 °C for traditional plane tool, but it does only about 500 °C for micro-grooved tool. Moreover, the cutting temperature decreases and the shear angle increases with decreasing micro-groove depth except for the case of 7 μm in micro-groove depth. The 25-μm-depth micro-grooved tool decreases cutting temperature and cutting force more greatly in larger material removal rate turning. In the dry turning with a micro-grooved tool, it is required that the micro-groove width is less than cutting chip width and its aspect ratio is enough large to maintain the air spaces between chip back surface and tool rake surface.

© 2013 Elsevier Ltd. All rights reserved.

1. Introduction

Titanium alloy has been widely applied in chemical, surgical, and aerospace industries, but its application was limited by high machining cost due to its poor machinability. This is because the strong friction between tool rake face and cutting chip produces large amounts of process heat, which will be focused on the tool-chip interface due to the poor thermal conductivity [1]. In order to reduce the friction on tool-chip interface, cryogenic cooling has been applied in machining titanium alloys [2]. Liquid nitrogen (LN_2) or carbon dioxide (CO_2) was also regarded as a coolant to improve tool life in machining of titanium alloy Ti-6Al-4 V [3]. However, the careless handling of liquid nitrogen and carbon dioxide snow could lead to cold burns and asphyxiation to person.

Recently, the dry machining of titanium alloy without any coolant has been receiving increasing attention. For example, the uncoated and CVD-coated carbide tools have good possibility to use in dry end milling of titanium alloy [4]. Moreover, the dry machining was carried out with uncoated carbide tools in finish operations [5]. However, these researches have not yet

significantly improved dry machining performance of titanium alloy. This is because a tool-chip adhesion exists in dry cutting.

In order to decrease the friction coefficient on tool rake face, some micron-scale textures were proposed on tool rake surface. For example, the micro-grooved tool with 0.10–0.15 μm in depth decreased chip adhesion to tool surface in wet cutting, but it increased the adhesion in dry cutting [6]. When the micro-grooved tool with 0.5–1.2 μm in depth was coated with TiN, it decreased the friction coefficient in dry cutting as same as in wet cutting [7]. It was, further, reported that the developed micro-grooved tool with 5-μm-depth micro-grooves parallel to cutting edge improved the anti-adhesive properties in dry cutting [8]. However, the above-mentioned researches only concerned the workpiece of aluminum alloy.

As for cutting force, the micro-grooved tool with 7.5 μm in depth decreased cutting force in wet milling of die steel NAK80 of HRC 40 [9]. Although the DLC-coated micro-grooved tool with 1.3 μm in depth may greatly decrease cutting force, the none-coated micro-grooved tool was not effective [10]. In dry machining of an aluminum alloy, a TiN coated micro-grooved tool with 0.5–1.2 μm in depth may be employed to decrease the cutting force [7]. However, until now their cutting temperature has not been investigated.

The orientation of micro-grooves on tool rake surface has controversially been discussed. In wet cutting of aluminum alloy

^{*} Corresponding author. Tel.: +86 20 87114634; fax: +86 20 87111038.
E-mail addresses: jinxie@scut.edu.cn, jxie25@hotmail.com(J. Xie).

using a DLC-coated micro-grooved tool with 1.5 μm in depth and 0.15 in aspect ratio, the micro-groove orientation vertical to chip flowing (parallel to cutting edges) decreased cutting force, but the one parallel to chip flowing (vertical to cutting edges) was not effective [11]. In both case of the micro-groove orientations vertical and parallel to chip flowing, the DLC-coated micro-grooved tools with 1 μm in depth and 20–25 μm in width decreased friction force and friction coefficient in wet cutting of aluminum alloy [7].

In the case of non-coated micro-grooved tool with 7.5 μm in depth, the micro-groove orientation parallel to chip flowing (vertical to cutting edges), however, produced much less cutting force than one vertical to chip flowing (vertical to cutting edges) in end milling of die steel [9]. It is not identical to the results of DLC-coated micro-grooved tool in turning of aluminum alloy [7,11]. For the non-coated micro-grooved tool with about 155 μm in micro-groove depth and about 0.43 in aspect ratio, the micro-grooves along chip flowing on tool rake surface also produced the best cutting performance in dry cutting of titanium alloy [12]. Hence, there could exist different chip lubrication behavior between micron-scale size and nanometer-scale size of micro-grooves on tool rake surface.

The micro-groove size on tool rake surface was also focused in cutting process. For example, the micro-grooved TiAlN-coated tool with 5 μm in depth and 0.25 in aspect ratio may significantly improve wear resistance and surface lubricity, but it was not effective with 0.1–0.15 μm in micro-groove depth and about 0.18 in aspect ratio [13]. It was also found that the cutting force increased with increasing micro-groove depth from 0.4 μm to 5 μm in wet cutting using a DLC coated micro-grooved tool [11]. Until now, the changes of cutting force with micro-groove depth have not been investigated when the micro-groove depth is larger than 10 μm .

The fabrication of micro-grooves on tool surface required a femto-second laser technology [8,11,13], a focused ion beam system [9] or a chemical etching through UV exposure [7]. Unfortunately, their micro-groove depths applied for micro-grooved tools were less than 10 μm due to the limitation of these micro-machining approaches. Hence, a diamond wheel V-tip was employed to fabricate a micro-grooved tool with about 155 μm in depth for dry turning of titanium alloy [12], but cutting temperature and cutting force were not investigated.

In this paper, various non-coated micro-grooved tools with 7–149 μm in depth are proposed on tool rake surfaces in dry cutting of titanium alloy. The objective is to understand how the micro-groove profile and size influence cutting temperature and cutting force with regard to different turning conditions. First, a diamond

grinding wheel was employed to fabricate accurate and smooth micro-groove arrays on tool rake surfaces; then the dry turning experiments of titanium alloy were performed using these micro-grooved tools; finally, cutting temperature, cutting force, chip formation and tool wear were investigated in connection with the micro-groove depth and material removal rate.

2. Micro-grinding of micro-grooves on tool rake surface

Fig. 1 shows CNC mutual-wear truing of diamond wheel V-tip. Before micro-grinding of micro-grooves on tool rake surface, the diamond grinding wheel profile was trued to be a V-tip. In truing experiment, a metal-bonded #600 diamond grinding wheel was employed. The wheel axial section was gradually trued into a V-tip profile through a mutual-wearing between the rotary diamond wheel and the fixed GC dresser along the V-shape tool paths [14]. The wheel V-tip angle α was controlled by the angle of crossed tool paths. The detailed truing conditions such as the wheel rotate speed N , the feed speed v_f , the depth of cut a , etc. are shown in Table 1.

Fig. 2 shows micro-grinding of micro-grooves on tool rake surface. In experiments, carbide blades (YG8) were chosen as cutting tools. In micro-grinding of micro-groove array on tool rake surface, the sharpened diamond wheel V-tip was employed with the wheel rotate speed N , the feed speed v_f and the depth of cut a (see Fig. 2a). The micro-groove orientation with an angle β of 45° to cutting edge was nearly identical to chip flow direction [12]. Moreover, the on-machine truing was performed before each grinding process to maintain the sharpness of grinding wheel V-tip. After the rough grinding, a fine grinding was performed by controlling the depth of cut from 5 μm to 1 μm so as to smooth

Table 1

CNC truing conditions of diamond wheel V-tip.

| CNC grinder | SMRART B818 |
|------------------------|---|
| Diamond grinding wheel | SD600, Metal-bonded, $N=2000\text{--}3000 \text{ rpm}$ $D=160 \text{ mm}$ |
| GC dresser | #180 GC → #600 GC $b=50, w=6 \text{ mm}$ |
| CNC Tool paths | V-shaped linear interpolation movement |
| Truing parameters | $v_f=200\text{--}100 \text{ mm/min}$ $a=20\text{--}2 \mu\text{m}/ \Sigma a=10 \mu\text{m}$ |
| Coolant | Water |

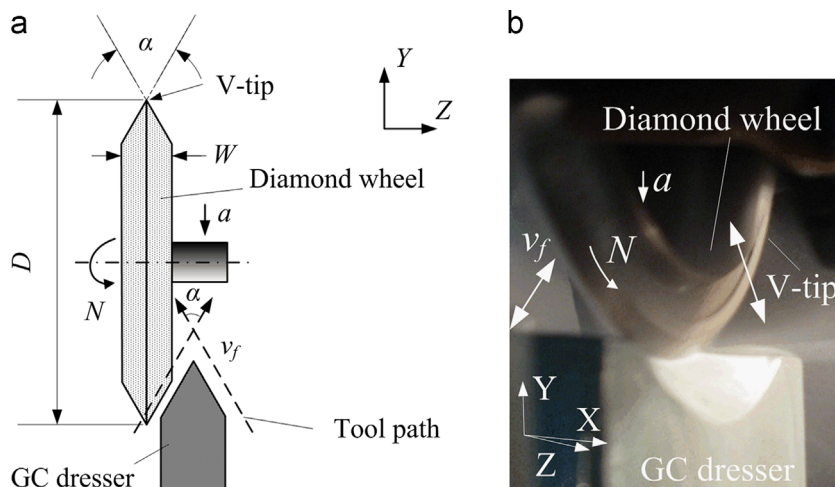


Fig. 1. CNC mutual-wear truing of diamond wheel V-tip: (a) truing principle and (b) truing scene.

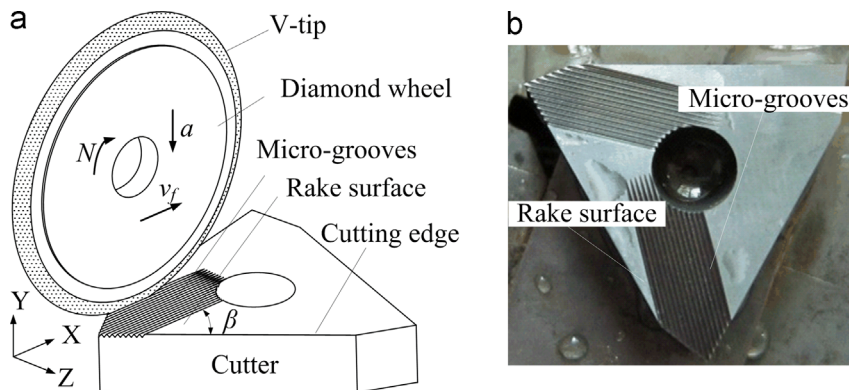


Fig. 2. Fabrication of micro-grooves on tool rake surface through the micro-grinding with a diamond wheel V-tip: (a) micro-grinding scheme and (b) ground micro-grooved tool.

Table 2
Micro-grinding conditions of micro-grooves on tool rake surface.

| CNC grinder | SMRART B818 |
|------------------------|--|
| Diamond grinding wheel | SD600, metal-bonded, $N=3538$ rpm |
| Workpiece | Carbide tool YG8 |
| Rough grinding | $v_f=1500$ mm/min, $a=5\ \mu\text{m}$ |
| Fine grinding | $v_f=200$ mm/min, $a=1\ \mu\text{m}$, Spark-out=2 |
| Coolant | Water |

micro-grooves surface. The detailed micro-grinding conditions are showed in Table 2.

3. Micro-groove profile shape and size

Fig. 3 shows SME topographies and section profiles on the rake surfaces of various micro-grooved tools. In this study, five micro-grooved tools were fabricated with different micro-groove profiles and sizes. The micro-ground micro-grooves were measured by using a white light interferometer BMT SMS Expert 3D. The measuring orientation was vertical to tool rake surface and micro-groove orientation. It is shown that the micro-grinding may produce a smooth surface and an accurate profile with little cracks. In contrast, the laser machining produced rough surface and profile of micro-grooves on tool rake surface [11,13].

Micro-groove depth h_v , aspect ratio γ_v , micro-groove angle α_v , and micro-groove tip radius r_v were regarded as micro-groove profile parameters. Moreover, the micro-groove error PV_v was considered to evaluate the micro-groove accuracy [12]. The measured results are shown in Table 3. It is shown that the micro-groove depth h_v , the micro-groove angle α_v and the aspect ratio γ_v ranged 7–149 μm , 77.4–137.9° and 0.14–0.50, respectively. The micro-groove error PV_v ranged 5.90–7.98 μm for micro-groove depth h_v of 53–149 μm . This means that a decrease in micro-groove depth h_v led to a decrease in aspect ratio γ_v and an increase in micro-groove error PV_v . This is because an arc radius existed on micro-groove bottom due to the difficulty of sharpening a diamond wheel V-tip and its tip wear in micro-grinding.

4. Dry turning experiments

Fig. 4 shows the scheme of dry turning of titanium alloy. A cemented carbide cutter (YG8, 31303C) was employed. The geometrical parameters of cutter were given by rake angle γ_0 of 0°, clearance angle α_0 of 0°, cutting edge angle K_r of 90°, minor cutting edge angle K_r' of 8°, and cutting edge inclination λ_s of 0°. All experiments were performed without any coolant. A titanium

alloy (Ti-6Al-4V) was chosen as workpiece. The detailed turning conditions such as the depth of cut a_p , the cutting speed v and the feed rate f are showed in Table 4.

In order to evaluate the cutting ability of micro-grooved tool, the material removal rate η was considered. Because of the tool cutting edge angle K_r of 90° and tool cutting edge inclination λ_s of 0°, the η is calculated as follows:

$$\eta = f a_p \cdot v \cdot 1000 \quad (1)$$

In the first experiment, the depth of cut a_p of 0.5 mm, cutting speed v of 49 m/min and feed rate f of 0.1 mm/r were employed to compare the cutting temperature between micro-grooved tool and traditional plane tool. The material removal rate η was 2450 mm^3/min .

In the second experiment, the depth of cut a_p of 0.5 mm, cutting speed v of 47 m/min and feed rate f of 0.1 mm/r was employed to observe the cutting temperature with regard to micro-groove depths. The material removal rate η was 2350 mm^3/min .

In the third experiment, much less material removal rate η of 360 mm^3/min and much larger material removal rate η of 11,700 mm^3/min were employed using $a_p=0.1$ mm, $v=36$ m/min and $f=0.1$ mm/r and $a_p=1.0$ mm, $v=39$ m/min and $f=0.3$ mm/r, respectively. The former was about 30 times less than the latter. The objective was to observe how the material removal rate influences cutting temperature and cutting force with different turning conditions.

5. Measurement of cutting temperature and cutting force

Fig. 5 shows the design of thermocouples installation for measuring temperature. It is very difficult to precisely measure cutting tip temperature in turning, thus the rake surface temperature was regarded as cutting temperature in this study. In order to measure the rake surface temperature, the thermocouples were installed in blind holes below tool rake surface with 0.6 mm distance to tool rake surface (see Fig. 5a). Three thermocouples were installed inside the mounting holes to measure temperatures of Points A, B and C on tool rake surface so as to investigate heat transfer. The mounting holes were fabricated using micro-hole ECD machine tool. Moreover, the throughout channels with 0.8 mm in depth were fabricated on tool back surface to guide the wires of thermocouples (see Fig. 5b).

In order to understand the relationship between cutter tip temperature and rake surface temperature, the temperatures of cutter tip and tool rake surface were measured before truing experiments. In measurement, the origin of heat was designed on cutter tip, which was heated by an electric iron without any

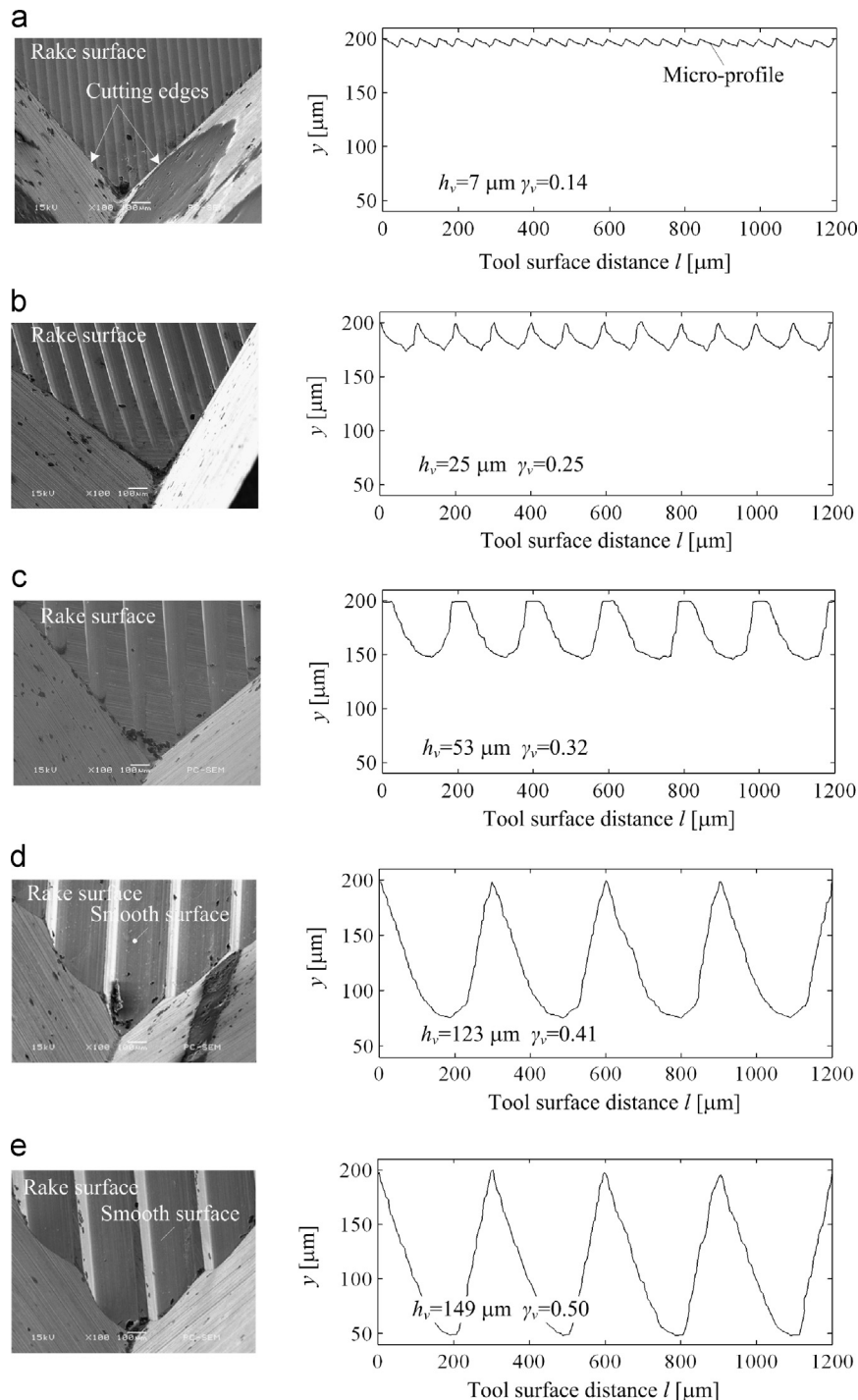


Fig. 3. Micro-topographies and micro-profile sizes of micro-grooved tools versus micro-groove depth h_v and aspect ratio γ : (a) $h_v=7 \mu\text{m}$, (b) $h_v=25 \mu\text{m}$, (c) $h_v=53 \mu\text{m}$, (d) $h_v=123 \mu\text{m}$ and (e) $h_v=149 \mu\text{m}$.

Table 3

The micro-groove profile parameters on tool rake surface.

| Depth (h_v , μm) | Width (w_v , μm) | Interval (δ_v , μm) | Aspect ratio (γ_v) | Angle (α_v , deg) | Tip radius (r_v , μm) | Form error (PV_v , μm) |
|---------------------------------|---------------------------------|---|-----------------------------|---------------------------|--------------------------------------|---------------------------------------|
| 7 | 50 | 50 | 0.14 | 137.90 | 7.0 | – |
| 25 | 100 | 100 | 0.25 | 126.22 | 22.3 | – |
| 53 | 160 | 200 | 0.32 | 77.94 | 43.1 | 5.90 |
| 123 | 300 | 300 | 0.41 | 77.42 | 66.7 | 8.75 |
| 149 | 300 | 300 | 0.50 | 77.37 | 50.2 | 7.98 |

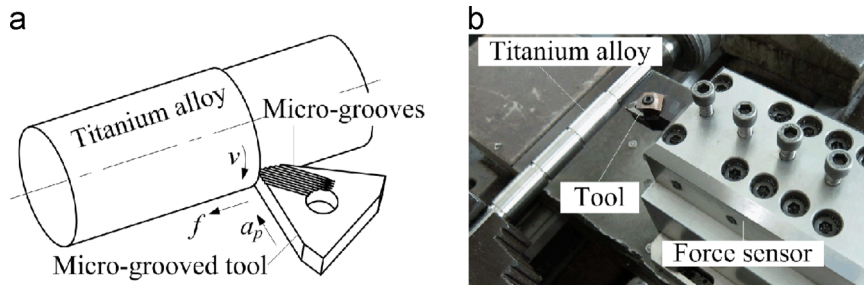


Fig. 4. Dry turning of titanium alloy using micro-grooved tool: (a) dry turning scheme and (b) dry turning scene along with force sensor.

Table 4
Turning conditions of titanium alloy.

| Turning machine | CK6136i |
|--------------------|---------------------------|
| Workpiece | Titanium alloy Ti-6Al-4 V |
| Depth of cut a_p | 0.1–1.0 mm |
| Cutting speed v | 36–49 m/min |
| Feed rate f | 0.1–0.3 mm/r |
| Coolant | In air |

cutting (see Fig. 5c). The objective is to predict the temperature of cutter tip through rake surface temperatures in turning process.

Moreover, a Kistler force sensor was employed to measure the cutting forces (see Fig. 4b). In this study, the cutting force was regarded as the resultant force of three component forces in the turning process. Because cutting temperature and cutting force are related to the cutting chip formation, the shearing angle θ was investigated. The θ is described as follows:

$$\theta = \tan^{-1} \frac{h \cos \gamma_0}{h_c - h \sin \gamma_0} \quad (2)$$

where h is the actual depth of cut. In this experiment, the h is equal to the feed rate f in the cases of tool parameters: the tool cutting edge angle K_r of 90° and tool cutting edge inclination λ_s of 0°. h_c is cutting chip thickness. In the measurement of cutting chip thickness, the saw-tooth height on chip free surface was removed away.

6. Results and discussions

6.1. Relationship between cutter tip temperatures versus rake surface temperatures

Fig. 6 shows cutter tip temperature versus rake surface temperature. It is shown that the rake surface temperatures at Point A, Point B and Point C increased with increasing the cutter tip temperature (see Fig. 6a). Moreover, they converged to the stable value when the cutting tip temperature reached a constant value at the same time. As a result, the rake surface temperatures at Point A, Point B and Point C responded to cutter tip temperature.

In order to understand the relationship between cutter tip temperature and surface temperatures, the changes of cutter tip temperature were investigated in connection with the rake surface temperatures for traditional plane tool and micro-grooved tool, respectively. It is seen that the cutter tip temperatures increased in logarithmic form with rake surface temperatures both for plane tool and micro-grooved tool: their correlations (R^2) were very good (see Fig. 6b). Hence, the cutting temperature T_t^* at cutter tip may be predicted by the rake surface temperatures according to these fitted logarithmic form curves.

It is also found that at the same cutter tip temperature, the micro-grooved tool produced larger rake surface temperatures at

Point A, Point B and Point C than traditional plane tool, respectively. Moreover, it also produced larger temperature grade along Point A, Point B and Point C. This means that the micro-grooves on tool rake surface transferred cutting heat along micro-groove orientation from cutting tip more rapidly than traditional plane tool. This contributes to excluding cutting heat from cutter tip.

6.2. Comparison of micro-grooved tool and traditional plane tool

Fig. 7 shows cutting temperature curves for micro-grooved tool and traditional plane tool. The micro-groove depth h_v for this micro-grooved tool was 53 μm. In dry turning, the depth of cut a_p was 0.5 mm. It is shown that the cutting temperature T greatly increased with cutting time t in both cases of traditional plane tool and micro-grooved tool (see Fig. 7a). After $t=120$ s, the cutting temperature T gradually converged to stable values of 191.5 °C at Point A, 161.7 °C at Point B and 146.5 °C at Point C for micro-grooved tool, respectively, but the cutting temperature T continued to increase for traditional plane tool. This is because the micro-grooves on tool rake surface may exclude cutting heat from cutting area more rapidly than traditional plane tool (see Fig. 6b).

It is also seen that the micro-grooved tool decreased the cutting temperatures at Points A, B and C by 35.1%, 33.5% and 34.2% at $t=127$ s compared with the traditional plane tool, respectively. It decreased the cutting temperature T at Point A near cutting tip by 103.6 °C (see Fig. 7a). According the fitted logarithmic form curve of cutting tip temperature and rake surface temperatures (see Fig. 6b), the predicted cutting tip temperature T_t^* was achieved by using measured rake surface temperatures on Point A, Point B and Point C. It is shown that in the case of traditional plane tool, the cutting tip temperature T_t^* reached about 1322 °C at $t=127$ s, but it did only about 500 °C in the case of micro-grooved tool (see Fig. 7b). It indicates that the cutter tip temperature may be reduced may reduce by about 62% using the micro-grooved tool instead of traditional plane tool.

Fig. 8 shows the SEM micro-topographies of cutting chips for micro-grooved tool and traditional plane tool. It is seen that the micro-grooved tool produced finer saw-tooth on chip free surface than traditional plane tool, leading to more stable cutting state. Moreover, it produced thinner cutting chip. Using Eq. (2), its shearing angle θ became larger, leading to less cutting force. It is identical to the results of dry turning titanium alloy using the 155-μm-depth micro-grooved tool [12]. This may also explain why the micro-grooved tool greatly decreased cutting temperature.

6.3. Cutting temperature and chip micro-topography versus micro-groove depth

Fig. 9 shows cutting temperature curves versus micro-groove depth h_v . The micro-groove depth ranged 7–149 μm. It is shown that the cutting temperature T decreased with decreasing micro-groove depth h_v from 149 μm to 25 μm. However, the cutting temperature T of $h_v=7$ μm was larger than the ones of $h_v=25$ μm

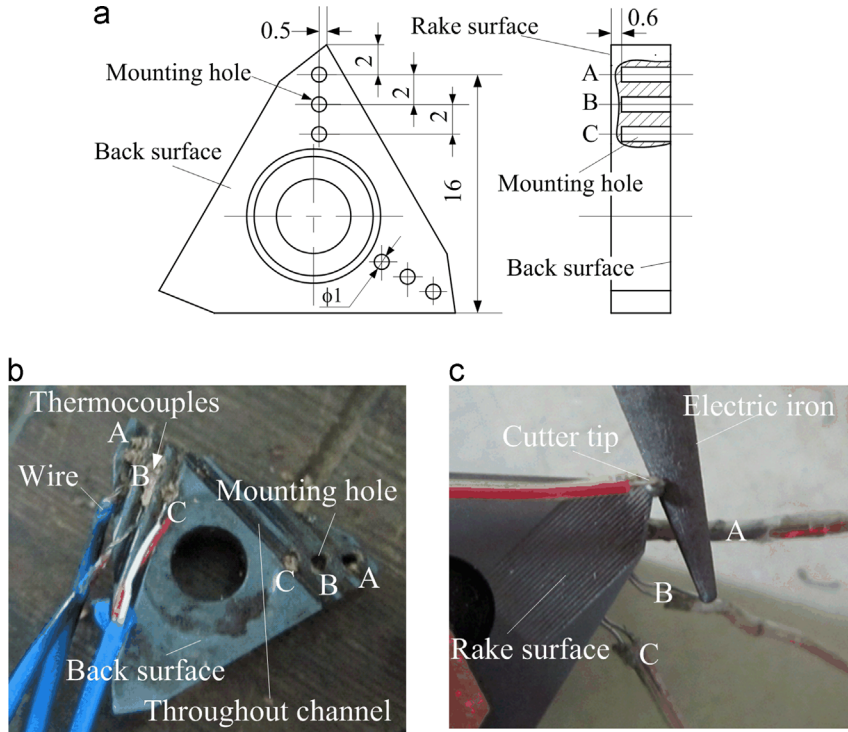


Fig. 5. Thermocouples installation for measuring cutting temperature: (a) mounting holes design, (b) thermocouples installation and (c) measuring setup of cutter tip.

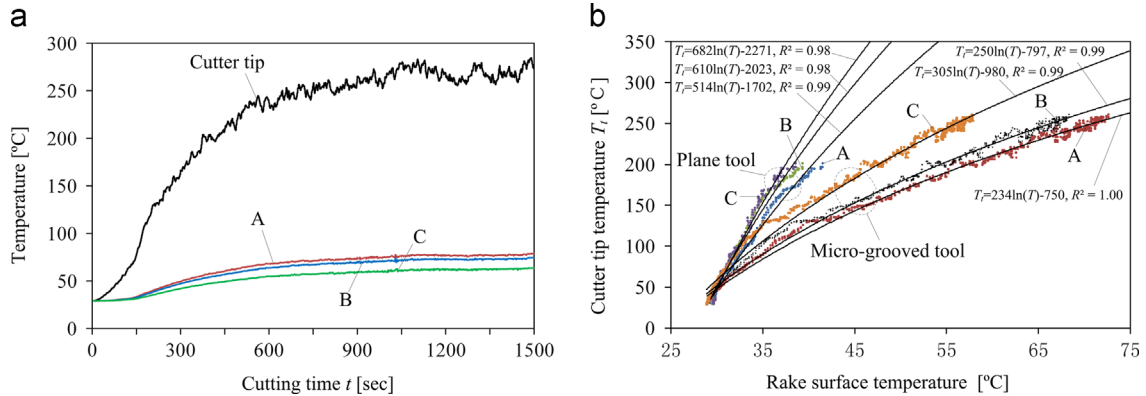


Fig. 6. Measurement of cutter tip temperature without turning: (a) temperature curve for micro-grooved tool and (b) cutter tip temperature T_t versus rake surface temperatures.

and $h_v=53\text{ }\mu\text{m}$. As a result, the 25- μm -depth micro-grooved tool produced the least cutting temperature. It is not identical to that the 100–200-nm-depth non-coated micro-grooved tools increased chip adhesion in dry cutting [9]. This is because the micro-groove surface ground by a diamond wheel V-tip was much smooth than the one fabricated by a laser machining (see Fig. 3).

Fig. 10 shows the cutting chip micro-topographies versus micro-groove depth h_v . It is seen that the micro-grooves were patterned on chip back surface by the micro-grooves on tool rake surface in turning process. The micro-groove size on chip back surface increased with increasing micro-groove depth h_v . Moreover, the 25- μm -depth micro-grooved tool produced the least saw-tooth phenomenon, leading to the best cutting stability. It is identical to the changes of cutting temperature with micro-groove depth (see Fig. 9). This is because less micro-groove width produced less contact area between chip back surface and tool rake surface, leading to fewer frictions. In the case of 7 μm in micro-groove depth, the contact area became large because its aspect ratio of 0.14 was very little (see Table 3).

In the cases of $h_v=123\text{ }\mu\text{m}$ and $h_v=149\text{ }\mu\text{m}$, the micro-grooved tools with 66.7 μm and 50.2 μm in micro-groove tip radius produced the same cutting temperature (see Fig. 9). Hence, the sharpness of micro-groove tip has little influence on cutting temperature. This is because the cutting chip did not reach the micro-groove bottom when the aspect ratio was enough large. This also means that there existed the air spaces between chip back surface and tool rake surface. This contributes to reducing the frictions between chip back surface and tool rake surface.

Fig. 11 shows shearing angle θ versus micro-groove depth h_v . The shearing angle θ was calculated through the measured chip thickness using Eq. (2). It is shown that shearing angle θ gradually increased when the micro-groove depth h_v was decreased from 149 μm to 25 μm , but the shearing angle of $h_v=7\text{ }\mu\text{m}$ was less than the ones of $h_v=25\text{ }\mu\text{m}$ and $h_v=53\text{ }\mu\text{m}$. Hence, the 25- μm -depth micro-grooved tool produced the largest shearing angle, leading to the least chip deformation and the least heat generation. It is identical to the changes of cutting temperature with micro-groove depth (see Fig. 9).

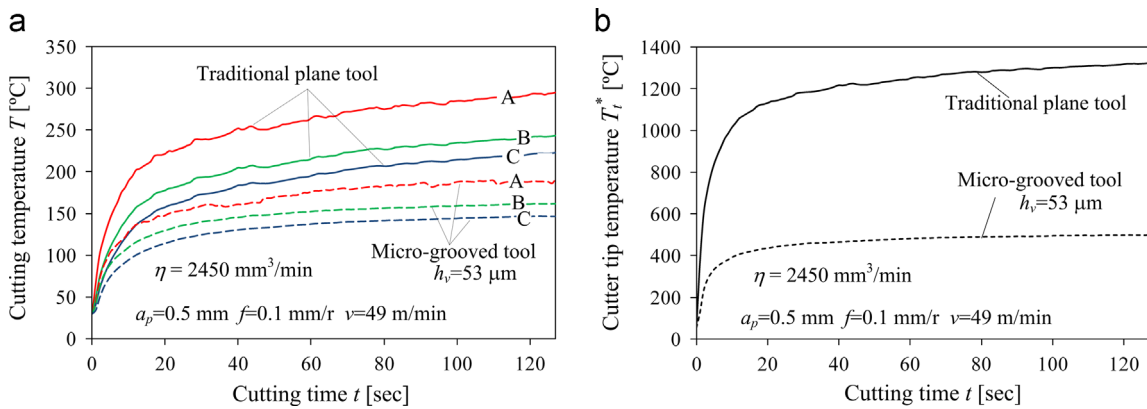


Fig. 7. Cutting temperatures for traditional plate tool and micro-grooved tool: (a) the cutting temperature T on tool rake surface and (b) the predicted cutter tip temperature T_t .

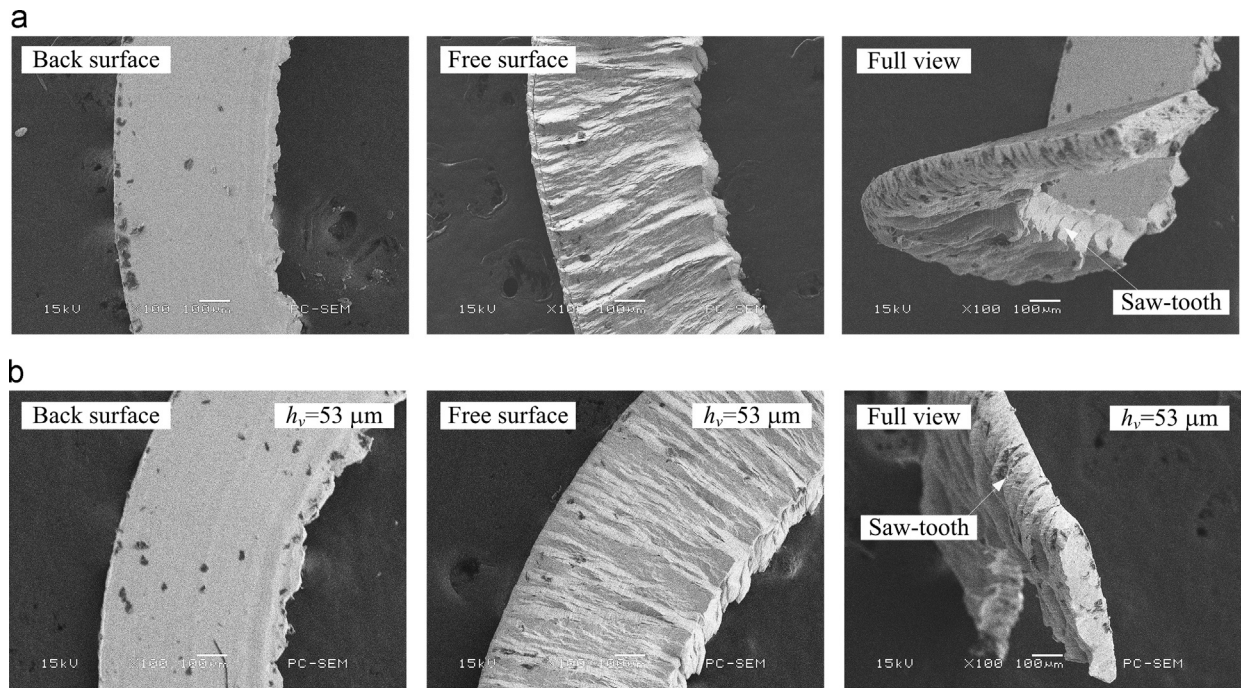


Fig. 8. Cutting chip micro-topographies: (a) traditional plane tool and (b) micro-grooved tool.

6.4. Cutting temperature and cutting force versus material removal rate

Fig. 12 shows the cutting temperature curves versus material removal rate η . It is shown that in the case of much less material removal rate of $\eta = 360 \text{ mm}^3/\text{min}$, the 25- μm -depth micro-grooved tool decreased cutting temperature T by 20.0% compared with traditional plane tool, but the 123- μm -depth micro-grooved tool increased cutting temperature T by 26.4% (see Fig. 12a). In the case of much larger material removal rate of $\eta = 11,700 \text{ mm}^3/\text{min}$, the 123- μm -depth and 123- μm -depth micro-grooved tools, however, both decreased cutting temperature by 27.2% and 21.8%, respectively (see Fig. 12b). This means that the micro-grooved tool decreased cutting temperature in large material removal rate turning.

Fig. 13 shows the cutting force versus material removal rate η . It is shown that in the case of much less material removal rate of $\eta = 360 \text{ mm}^3/\text{min}$, the 25- μm -depth micro-grooved tool decreased cutting force by 32.7% compared with traditional plane tool, but the 123- μm -depth micro-grooved tool increased cutting force. In the case of much larger material removal rate of $\eta = 11,700 \text{ mm}^3/\text{min}$,

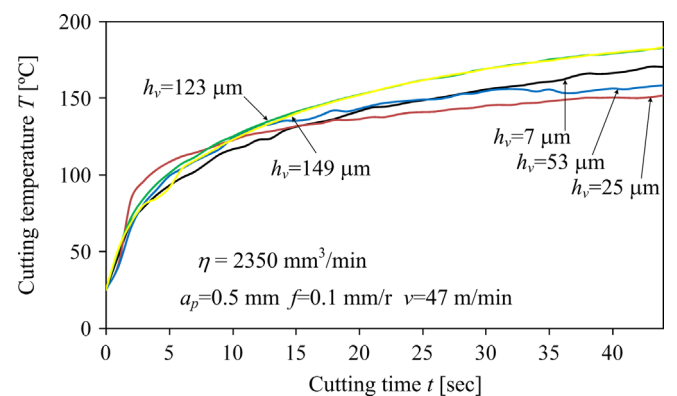


Fig. 9. Cutting temperature curves for micro-grooved tools with different micro-groove depth h_v .

the 25- μm -depth micro-grooved tool, further, decreased cutting force by 56.1%. In contrast, the 123- μm -depth micro-grooved tool decreased cutting force by 3.3%. It is identical to the changes of

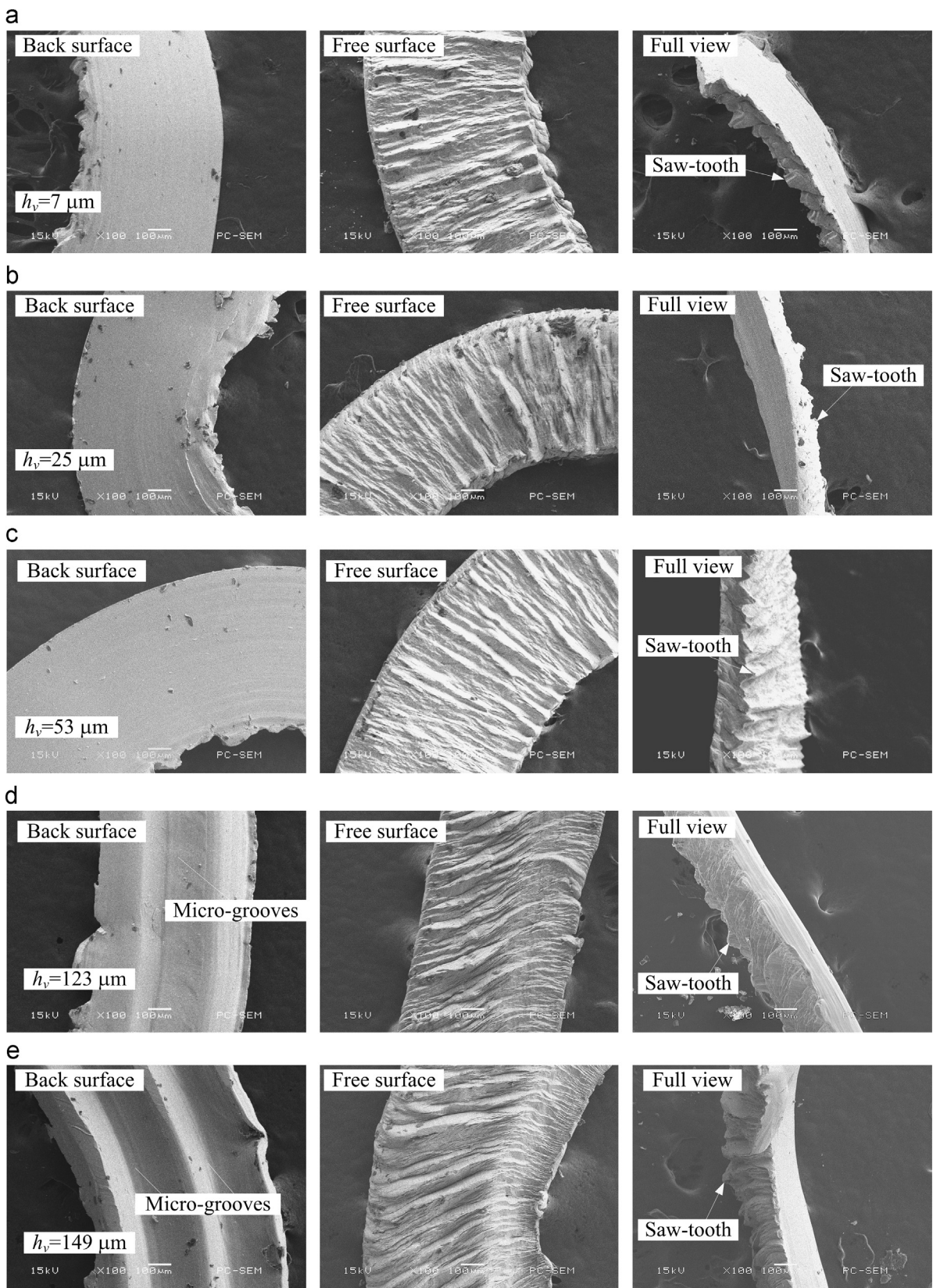


Fig. 10. Cutting chip micro-topographies for micro-grooved tools with different micro-groove depth h_v : (a) $h_v=7 \mu\text{m}$, (b) $h_v=25 \mu\text{m}$, (c) $h_v=53 \mu\text{m}$, (d) $h_v=123 \mu\text{m}$ and (e) $h_v=149 \mu\text{m}$.

cutting temperature (see Fig. 12). Hence, the micro-grooved tools may decrease cutting force in much larger material removal rate turning. This also means that a decrease in cutting force led to a decrease in cutting temperature (see Figs. 12 and 13).

This is because in the case of $\eta=360 \text{ mm}^3/\text{min}$, the cutting chip width including the depth of cut of $a_p=100 \mu\text{m}$ and chip deformation, was larger than the micro-groove width of $100 \mu\text{m}$ for $h_v=25 \mu\text{m}$. This would make cutting chip slide on micro-grooved

surface, leading to less cutting temperature and cutting force than traditional plane tool (see Figs. 12a and 13). In contrast, it was much less than the micro-groove width of 300 μm for $h_v=123 \mu\text{m}$, thus the cutting chip fell inside a micro-groove in turning. This would produce greater friction between cutting chip and micro-groove flanks, thus leading to larger cutting temperature and cutting force than traditional plane tool (see Figs. 12a and 13).

In the case of $\eta=11,700 \text{ mm}^3/\text{min}$, the cutting chip width with the depth of cut of $a_p=1000 \mu\text{m}$, however, was much larger than the micro-groove width both for $h_v=25 \mu\text{m}$ and $h_v=123 \mu\text{m}$. Hence, large material removal rate may make the cutting chip sliding on tool micro-grooved surface. It would reduce cutting chip adhesion and speed cutting chip flowing, leading to less cutting temperature and cutting force than traditional plane tool (see Figs. 12b and 13).

In comparison with traditional pate tool, the 25- μm -depth micro-grooved tool may decrease cutting temperature and cutting force more greatly in larger material removal rate turning. It is identical to the results that the non-coated micro-grooved tool decreased cutting force in wet turning only when the cutting speed was large [11] and the non-coated micro-grooved tool decreased drilling force only when the feed rate was large [10].

6.5. Cutting chip micro-topography versus material removal rate

Fig. 14 shows the SEM photos of cutting chip micro-topographies for much less material removal rate of $\eta=360 \text{ mm}^3/\text{min}$. It is shown that the 25- μm -depth micro-grooved tool produced less saw-tooth

on the chip free surface than traditional plane tool, leading to more stable cutting process. This may explain why the 25- μm -depth micro-grooved tool decreased cutting temperature and cutting force (see Figs. 12a and 13).

It is also found that two groove traces were patterned on chip back surface with burr edges for the 25- μm -depth micro-grooved tool. It indicates that the cutting chip was sliding on tool rake surface. In contrast, no groove traces existed on chip back surface with smooth edges for the 123- μm -depth micro-grooved tool. This is because the cutting chip fell inside the micro-groove valley on tool rake surface due to its micro-groove width larger than cutting chip width. This also made the burrs of chip edges removed by the micro-groove flanks in turning, thus leading to much great frictions. This may explain why the 123- μm -depth micro-grooved tool produced larger cutting temperature and cutting force than traditional plane tool (see Figs. 12a and 13).

Fig. 15 shows the SEM photos of cutting chip micro-topographies for much larger material removal rate of $\eta=11,700 \text{ mm}^3/\text{min}$. It is shown that there existed obvious micro-grooves on chip back surface with burr edges for both 25- μm -depth and 123- μm -depth micro-grooved tools. This is because the cutting chip width was much larger than their micro-groove widths in much larger material removal rate turning, thus leading to cutting chip sliding on the micro-grooves. When the cutting chip width was much less than the micro-groove widths for 123- μm -depth micro-grooved tools with $\eta=360 \text{ mm}^3/\text{min}$, the cutting chip, however, fell inside the micro-groove valley, leading to great frictions. This may explain why the 123- μm -depth micro-grooved tools produced less cutting

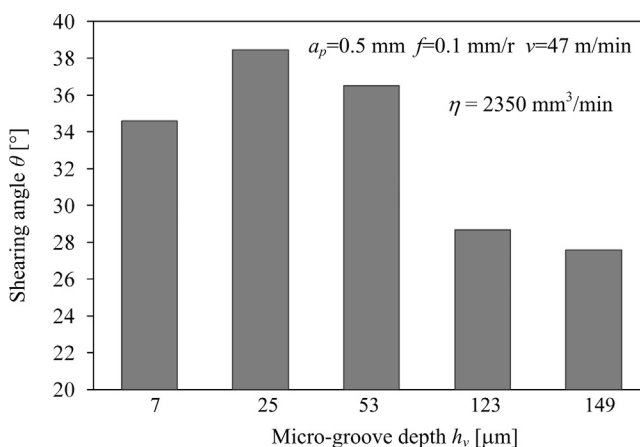


Fig. 11. Shearing angle θ for micro-grooved tool with different micro-groove depth h_v .

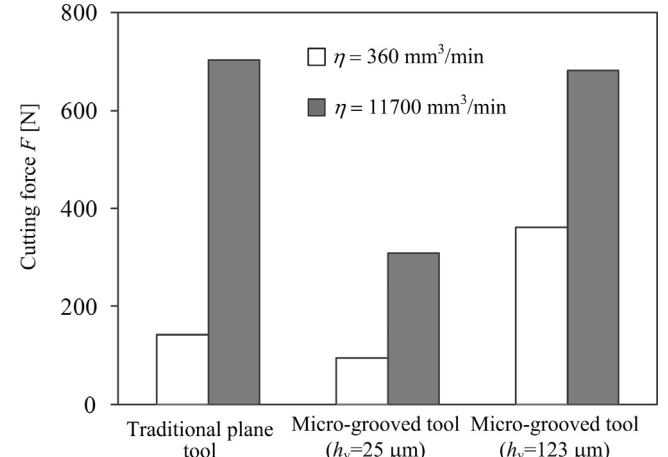


Fig. 13. Cutting force F versus material removal rate η for traditional plane tool and micro-grooved tools.

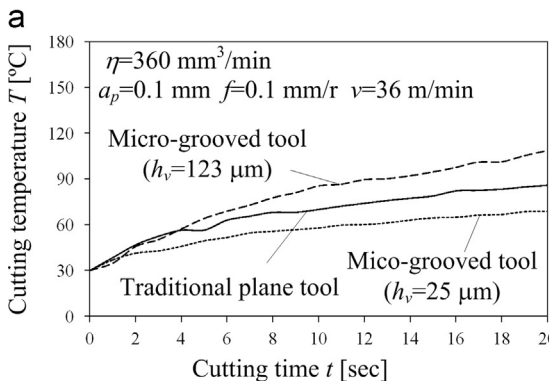
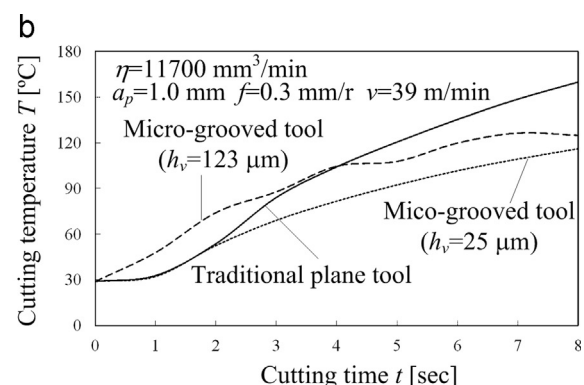


Fig. 12. Cutting temperature curves for traditional plane tool and micro-grooved tools: (a) $\eta=360 \text{ mm}^3/\text{min}$ and (b) $\eta=11,700 \text{ mm}^3/\text{min}$.



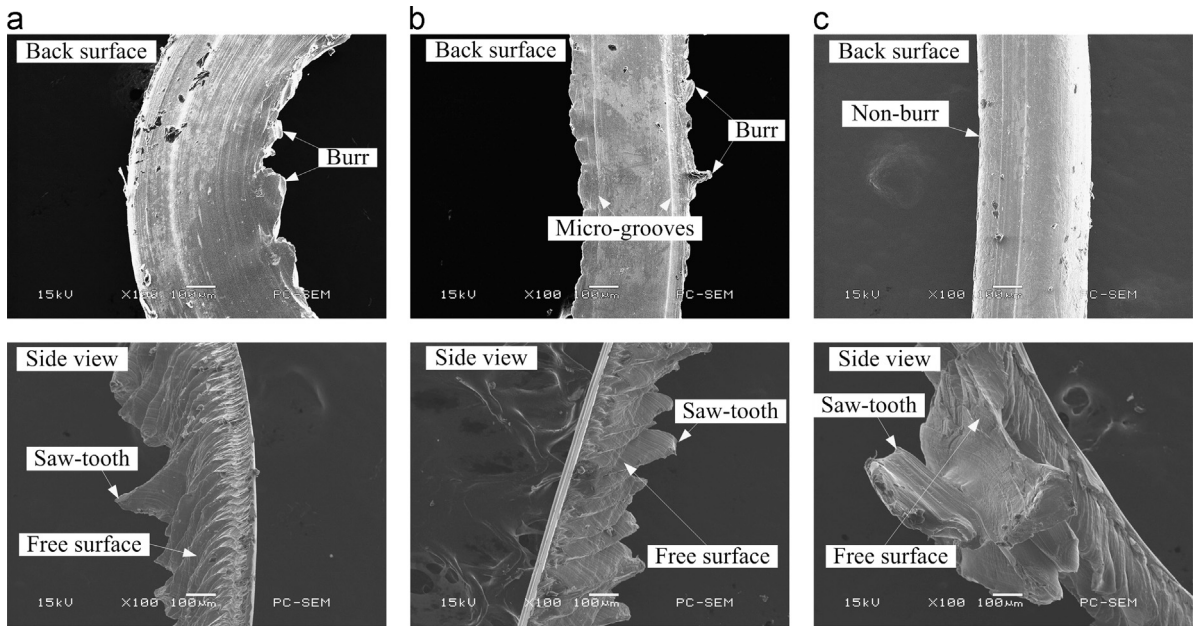


Fig. 14. Micro-topographies of cutting chips for $\eta=360 \text{ mm}^3/\text{min}$ and $a_p=0.1 \text{ mm}$: (a) traditional plane tool, (b) the 25- μm -depth micro-grooved tool and (c) the 123- μm -depth micro-grooved tool.

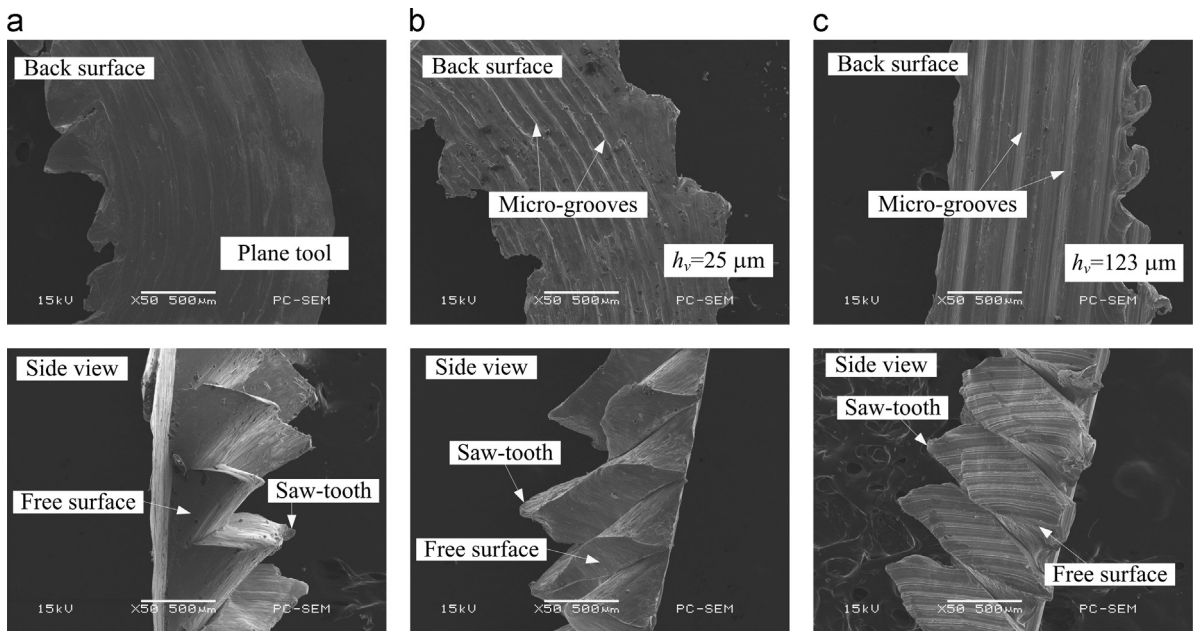


Fig. 15. Micro-topographies of cutting chips for $\eta=11700 \text{ mm}^3/\text{min}$ and $a_p=1.0 \text{ mm}$: (a) traditional plane tool, (b) the 25- μm -depth micro-grooved tool and (c) the 123- μm -depth micro-grooved tool.

temperature and cutting force than traditional plane tool only in much larger material removal rate turning (see Figs. 12 and 13).

Moreover, the 123- μm -depth micro-grooved tool produced much deeper micro-grooves on chip back surface than the 25- μm -depth micro-grooved tool in turning with $\eta=11,700 \text{ mm}^3/\text{min}$ (see Figs. 15c and 16). Although it might control cutting chip flowing, it led to much larger contact area between chip back surface and tool rake surface and much larger chip deformation. This may explain why the 123- μm -depth micro-grooved tool produced much larger cutting force than the 25- μm -depth micro-grooved tool (see Fig. 13).

Fig. 16 shows the cutting chip cross section for the 123- μm -depth micro-grooved tool in much larger material removal rate turning. It is showed that the micro-grooves with about 114 μm in depth were patterned on chip back surface by tool micro-grooves in turning process. This also means that there existed about 9- μm -depth air spaces between chip back surface and micro-groove valleys on tool rake surface. This contributes to reducing cutting chip adhesion and excluding cutting heat. This may explain why the 123- μm -depth micro-grooved tools produced much less cutting temperature than traditional plane tool in much larger material removal rate turning (see Fig. 12).

6.6. Tool wear

Fig. 17 shows the SEM photos of tool tip wear for traditional plane tool and micro-grooved tools. The tool tip wears were observed after all above-mentioned turning experiments. It is seen that the burn trace existed on tool rake surface for both traditional plane tool and 123-μm-depth micro-grooved tool (see Fig. 17a and c), but it was not found on the rake surface for the 25-μm-depth micro-grooved tool (see Fig. 17b). The reason is that the 25-μm-depth micro-grooved tool produced the least cutting temperature (see Figs. 12 and 13). Moreover, the burn trace appeared on the cutter tip for traditional plane tool, but it did on the rake surface for 123-μm-depth micro-grooved tool. This is because traditional plane tool without any micro-grooves had no way to exclude cutting chip and cutting heat rapidly, thus leading to much larger cutter tip temperature (see Fig. 7b).

It is also found that the 25-μm-depth micro-grooved tool produced the least worn area of cutter tip (see Fig. 17b). It is identical to the results that φ0.5-mm micro-grooved tool may improve drilling life [10]. Moreover, it produced the sharpest cutting edges of cutter after dry turning (see Fig. 17b). This is because its cutting temperature and cutting force were the least

(see Figs. 12 and 13). This also means that sharp cutting edges may reduce cutting temperature and cutting force.

7. Conclusions

- (1) The micro-grinding with a diamond wheel V-tip may fabricate smooth and accurate micro-grooves on tool rake surface. They produce the air spaces between cutting chip back and tool rake surface in dry turning of titanium alloy, thus leading to rapid cutting chip sliding. This contributes to excluding cutting chip and cutting heat.
- (2) The micro-grooved tool may decrease cutting temperature by 103 °C and more compared with traditional plane tool. According to the relationship between cutter tip temperature and rake surface temperatures, the predicted cutting tip temperature reaches about 1322 °C for traditional plane tool, but it did only about 500 °C for micro-grooved tool.
- (3) On decreasing micro-groove depth from 149 μm to 25 μm, cutting temperature decreases and shearing angle increases. However, cutting temperature greatly increases and shearing angle greatly decreases at the micro-groove depth of 7 μm and the aspect ratio of 0.14. This is because the aspect ratio is too little to form air spaces between cutting chip back and tool rake surface.
- (4) In little material removal rate, the 25-μm-depth micro-grooved tool may decrease cutting temperature and cutting force by 20.0% and 32.7% against traditional plane tool, respectively. In large material removal rate, it may, further, decrease cutting temperature by 27.2% and cutting force by 56.1%, respectively.
- (5) After all dry turning experiments, the 25-μm-depth micro-grooved tool produces the sharpest cutting edges and the least tool tip wear without any tool burn traces. This means that sharp tool cutting edges and little cutting tip wears contribute to the reductions of cutting temperature and cutting force.
- (6) In order to decrease cutting chip frictions and exclude cutting heat, the micro-groove depth needs to be large enough to maintain the air space between chip back surface and tool rake surface. Moreover, the micro-groove width needs to be less than cutting chip width so as to produce cutting chip sliding on tool rake surface.

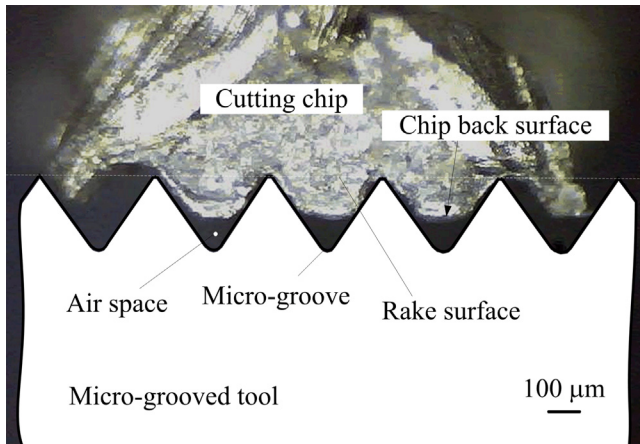


Fig. 16. Interface between tool rake surface and chip back surface for 123-μm-depth micro-grooved tool and $\eta=11,700 \text{ mm}^3/\text{min}$.

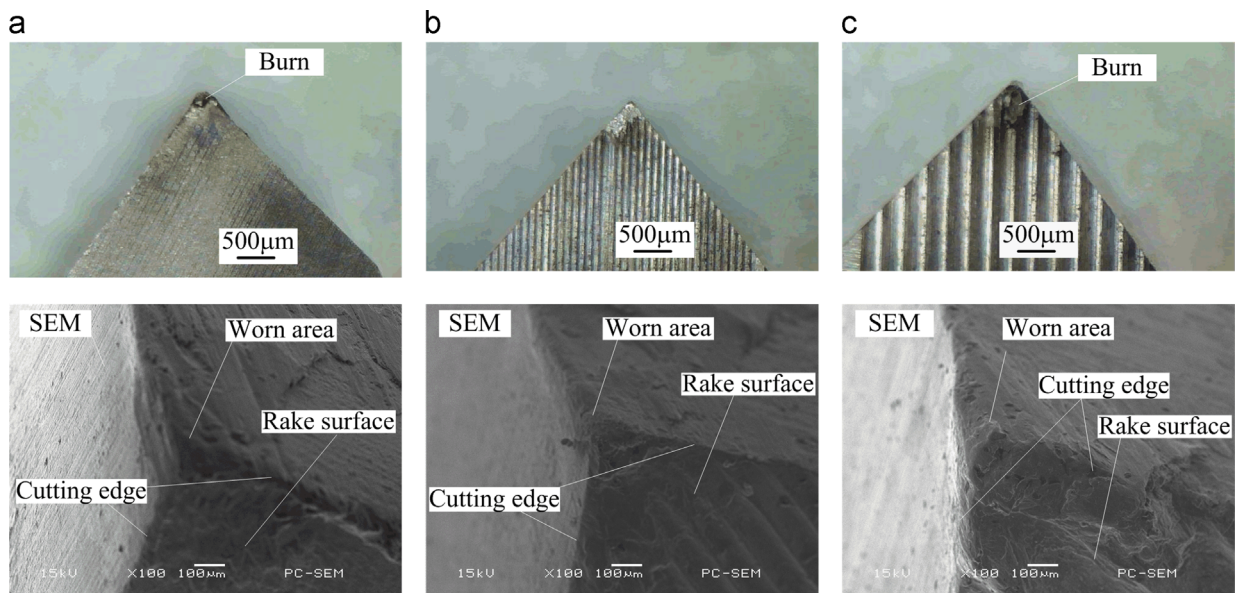


Fig. 17. Cutter tip wears after all turning experiments: (a) traditional plane tool, (b) the 25-μm-depth micro-grooved tool and (c) the 123-μm-depth micro-grooved tool.

Acknowledgments

The project was sponsored by the Natural Science Foundation of China (Grant no. 51075156).

References

- [1] M. Rahman, Y.S. Wong, A.R. Zareena, Machinability of titanium alloys, *JSME International Journal Series C* 46 (2003) 107–115.
- [2] S.Y. Hong, I. Markus, W.C. Jeong, New cooling approach and tool life improvement in cryogenic machining of titanium alloy Ti-6Al-4V, *International Journal of Machine Tools and Manufacture* 41 (2001) 2245–2260.
- [3] Christian Machai, Dirk Biermann, Machining of β -titanium-alloy Ti-10V-2Fe-3Al under cryogenic conditions: cooling with carbon dioxide snow, *Journal of Materials Processing Technology* 211 (2011) 1175–1183.
- [4] C.H.C. Haron, A. Ginting, H. Arshad, Performance of alloyed uncoated and CVD-coated carbide tools in dry milling of titanium alloy Ti-6242S, *Journal of Materials Processing Technology* 185 (2007) 77–82.
- [5] A. Ginting, M. Nouari, Surface integrity of dry machined titanium alloys, *International Journal of Machine Tools & Manufacture* 49 (2009) 325–332.
- [6] T. Sugihara, T. Enomoto, Development of a cutting tool with nano/micro-textured surface: Improvement of anti-adhesive effect by considering the texture patterns, *Precision Engineering* 33 (2009) 425–429.
- [7] Toshiyuki Obikawa, Akihiro Kamio, Hidemitsu Takaoka, Akira Osada, Microtexture at the coated tool face for high performance cutting, *International Journal of Machine Tools and Manufacture* 51 (2011) 966–972.
- [8] T. Sugihara, T. Enomoto, Improving anti-adhesion in aluminum alloy cutting by micro stripe texture, *Precision Engineering* 36 (2012) 229–237.
- [9] W.L. Chang, J.N. Sun, X.C. Luo, J.M. Ritchie, C. Mack, Investigation of microstructured milling tool for deferring tool wear, *Weal* 271 (2011) 2433–2437.
- [10] N. Kawasegi, H. Sugumori, N. Morita, Cutting tools with microscale and nanoscale textures, *Journal of the Japan Society for Abrasive Technology* 56 (2012) 665–668.
- [11] N. Kawasegi, H. Sugumori, H. Morimoto, N. Morita, I. Hori, Development of cutting tools utilizing surface functions induced by micro/nanometer-scale textures—turning experiments of aluminum alloy using DLC coated tools, *Journal of the Japan Society of Precision Engineering* 75 (2009) 1245–1249.
- [12] J. Xie, M.J. Luo, J.L. He, X.R. Liu, T.W. Tan, Micro-grinding of micro-groove array on tool rake surface for dry cutting of titanium alloy, *International Journal of Precision Engineering and Manufacturing* 13 (2012) 1845–1862.
- [13] T. Enomoto, T. Sugihara, S. Yukinaga, K. Hirose, U. Satake, Highly wear-resistant cutting tools with textured surfaces in steel cutting, *CIRP Annals—Manufacturing Technology* 61 (2012) 571–574.
- [14] J. Xie, Y.W. Zhuo, T.W. Tan, Experimental study on fabrication and evaluation of micro pyramid-structured silicon surface using a V-tip of diamond grinding wheel, *Precision Engineering* 35 (2011) 173–182.